

## **Real-time hybrid simulation based on vector form intrinsic finite element and FPGA**

Yuan-Feng Duan<sup>1)</sup>, Yi Fang<sup>2)</sup>, \*Jun-Jie Tao<sup>3)</sup>,  
Hong-Mei Zhang<sup>4)</sup>, and Chung-Bang Yun<sup>5)</sup>

<sup>1), 2), 4), 5)</sup> *College of Civil Engineering and Architecture, Zhejiang University,  
Hangzhou, China*

<sup>3)</sup> *Department of Civil & Mineral Engineering, University of Toronto, Ontario, Canada*

<sup>1)</sup> *ceyfduan@zju.edu.cn*

### **ABSTRACT**

Catching dynamic response of the complex structure accurately is crucial to reduce the disaster losses, which can be verified by testing methods. Real-time hybrid simulation (RTHS) is a quite powerful testing method by combining the numerical simulation and experimental testing. The numerical part is generally highly simplified to relieve the computation burden, which causes the deviation between numerical model and real structure, especially when the testing structure is complex and the numerical part has a large number of degrees of freedom. Moreover, Fine modeling may introduce time delays, resulting in the stability and accuracy of the RTHS. Thus, in this paper, a parallel RTHS platform is proposed for relieving the computation burden and realizing the real-time control, based on the vector form intrinsic finite element (VFIFE) and the field programmable gate array (FPGA). Two cases are carried out that prove the proposed RTHS platform can be well used to conduct the experimental research of RTHS, with accurate timing and high computation efficiency.

### **1. INTRODUCTION**

Hybrid simulation (HS) is a novel method to analyze the structural dynamic responses by combining numerical simulation with experimental analysis. In this method, the structure is divided into two parts: the components of the structure for which a reliable numerical model is not available are isolated and tested physically in the laboratory, while the rest of the system is modeled numerically. HS allows people to test only the components of interest rather than the entire structure. Therefore, compared with the traditional shaking-table test, HS can be applied to various structures regardless of the limitations on dimensions in a cost-effective manner.

Real-time hybrid simulation (RTHS) was introduced to analyze the structures with

---

<sup>1), 4), 5)</sup> Professor

<sup>2), 3)</sup> Graduate Student

rate dependent components which need to be conducted in real time (Nakashima 1992, Horiuchi 1999). A major challenge in RTHS is to run the numerical simulation as quickly as possible in terms of both algorithmic and hardware efficiency. Most existing RTHS are conducted by using highly simplified numerical models, with a few degrees of freedom (DOFs) and algorithms in a large-time step, to speed-up numerical simulation in an RTHS (Mercan 2009, Wu 2011). More research is needed to conduct an RTHS in a more refined numerical model containing more DOFs.

Vector form intrinsic finite element (VFIFE) is a structural analysis method proposed by Ting (2004a, 2004b) to handle nonlinear dynamic problems involving large deformations or rigid motions. Many studies on structural nonlinearity have been conducted using the VFIFE (Wu 2008, Wang 2011, Duan 2014). All these studies show that the VFIFE can provide accurate results for complex structural behavior in an efficient manner. The structure in VFIFE is modeled as a series of particles with mass interconnected by massless elements. Dynamic analysis is conducted based on each particle and element. No assembling is needed for global stiffness. Therefore, the VFIFE is highly flexible and suitable for implementation in parallel.

The FPGA is a kind of electronic chip equipped with many configurable logic blocks (CLBs). One of its merits is excellent performance in parallel computation. Moreover, it has exhibited impressive performance in deterministic timing and can artificially trigger its on-chip program at fixed-time intervals along the order of nanoseconds. It has been widely used in measurement and control engineering, which requires small latencies (Jung 2007), and has been applied to RTHS (Sorkhabi 2015).

In this paper, a parallel RTHS platform proposed taking advantage of the intrinsic independence of the VFIFE and the parallel computing capability of the FPGA. All programs, including numerical simulation part, programs for the external I/O, outer loop controller, and data acquisition, are designed in the uniform programming environment of LabVIEW and integrated on a FPGA-based device. An illustrative simple RTHS of a structure with three DOFs was executed to demonstrate the feasibility of the proposed parallel platform. A virtual RTHS was then run on a cable and damper system with 147 DOFs to show the promising computing capability of this parallel RTHS platform.

## **2. APPLICATION OF VFIFE TO RTHS**

### *2.1 VFIFE method*

The structure of the VFIFE is divided into a series of mass particles connected by massless elements. Each particle independently follows Newton's second law of motion. Thus, the governing equation for each particle with mass can be obtained as

$$\mathbf{M}\ddot{\mathbf{u}} = \mathbf{F} - \mathbf{f}, \quad (1)$$

where  $\mathbf{M}$  is the diagonal mass matrix of each particle, and  $\ddot{\mathbf{u}}$ ,  $\mathbf{F}$ , and  $\mathbf{f}$  denote the acceleration, applied external force, and internal force vectors of each. The internal force vector  $\mathbf{f}$  can be assembled from the associated elemental forces at each particle.

The procedure of the VFIFE can be mainly divided into prediction of particle displacements and evaluation of the elemental forces. Particle displacements are predicted using the central different method (CDM) as

$$\mathbf{u}_{n+1} = \mathbf{M}^{-1}(\mathbf{F}_n - \mathbf{f}_n)h^2 + 2\mathbf{u}_n - \mathbf{u}_{n-1} \quad (2)$$

$$\mathbf{u}_{-1} = \mathbf{u}_0 - h\dot{\mathbf{u}}_0 + \frac{1}{2}h^2\ddot{\mathbf{u}}_0 \quad (3)$$

where  $\mathbf{u}_{n-1}$ ,  $\mathbf{u}_n$ , and  $\mathbf{u}_{n+1}$  are the absolute particle displacement vectors at the previous, given, and next time step,  $\mathbf{u}_0$ ,  $\dot{\mathbf{u}}_0$ , and  $\ddot{\mathbf{u}}_0$  are relevantly for the initial time step.  $\mathbf{F}_n$  and  $\mathbf{f}_n$  are the external and internal force vectors at the given time step, and  $h$  is the time step. The calculation of  $\mathbf{f}_{n+1}$  is described by an example in Fig. 1. It concludes the elimination of rigid body translation and rotation ( $d$  and  $\theta$ ), the extraction of pure deformations ( $\Delta l$ ,  $\varphi^a$ , and  $\varphi^b$ ), and element forces calculation in the convected coordinates. In Fig. 1, superscripts  $a$  and  $b$  denote two ends of the beam element, and the subscripts  $n$  and  $n+1$  represent the given and the next time steps, respectively. More details can be found in the works of Ting (2004a).

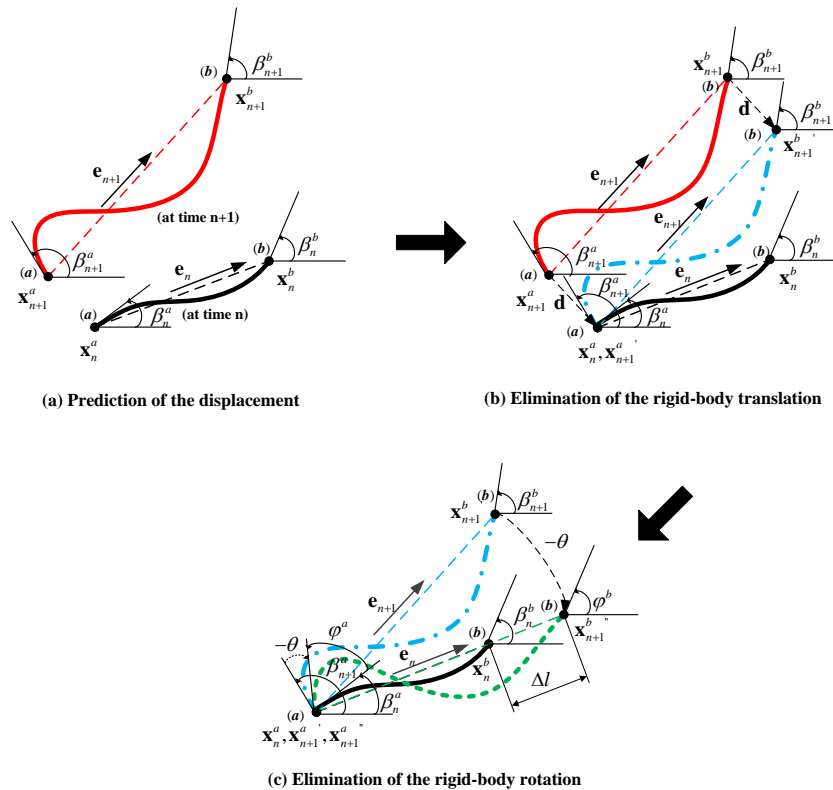


Fig. 1 Procedure of elemental force calculation for a plane beam element

The lengths of the element at different time steps ( $n$  and  $n + 1$ ) are given by

$$l_{n+1} = |\mathbf{x}_{n+1}^a - \mathbf{x}_{n+1}^b| \quad \text{and} \quad l_n = |\mathbf{x}_n^a - \mathbf{x}_n^b| \quad (4)$$

where  $\mathbf{x}$  is the translational component of particle displacement vector  $\mathbf{u}$ . Likewise, the rotational increments,  $\Delta\beta$ , between time steps are obtained by the difference of

rotation of the end of an element

$$\Delta\beta^a = \beta_{n+1}^a - \beta_n^a \quad \text{and} \quad \Delta\beta^b = \beta_{n+1}^b - \beta_n^b \quad (5)$$

The unit vector,  $\mathbf{e}_{n+1}$ , and rigid body rotational increment  $\theta$  can be obtained as

$$\mathbf{e}_{n+1} = \frac{1}{l_{n+1}} (\mathbf{x}_{n+1}^a - \mathbf{x}_{n+1}^b) \quad (6)$$

$$\theta = \cos^{-1}(\mathbf{e}_{n+1} \cdot \mathbf{e}_n) \quad (7)$$

The pure translational and rotational deformation,  $\Delta l$  and  $\phi$ , of the element are

$$\Delta l = l_{n+1} - l_n, \quad \phi^a = \Delta\beta^a - \theta, \quad \phi^b = \Delta\beta^b - \theta \quad (8)$$

With pure deformation,  $\Delta l$ ,  $\phi^a$ , and  $\phi^b$ , and the incremental element forces,  $\Delta f$ ,  $\Delta m^a$ , and  $\Delta m^b$  can be obtained as

$$\begin{bmatrix} \Delta f \\ \Delta m^a \\ \Delta m^b \end{bmatrix} = \frac{E}{l_n} \begin{bmatrix} A & 0 & 0 \\ 0 & 4I & 2I \\ 0 & 2I & 4I \end{bmatrix} \begin{bmatrix} \Delta l \\ \phi^a \\ \phi^b \end{bmatrix} \quad (9)$$

where  $\Delta f$ ,  $\Delta m^a$  and  $\Delta m^b$  are the increment in the elemental force along the axial direction, and increments in the elemental moments at two nodes, and  $I$  is the inertial moment of the beam cross-section. Then equations can be obtained as

$$\begin{aligned} \sum M = 0, \Delta f_y^b = \frac{1}{l_n} (\Delta m^a + \Delta m^b), \sum F_y = 0, \Delta f_y^a = -\Delta f_y^b, \sum F_x = 0, \Delta f_x^a = -\Delta f_x^b = -\Delta f, \\ \Delta \mathbf{f}^{a*} = [\Delta f_x^a, \Delta f_y^a, \Delta m^a]^T, \Delta \mathbf{f}^{b*} = [\Delta f_x^b, \Delta f_y^b, \Delta m^b]^T \end{aligned} \quad (10)$$

where the subscripts  $x$  and  $y$  mean the axial and vertical directions of the convected coordinates, respectively, and superscript  $*$  denotes the convected coordinates at the new time step  $n+1$ . Equation (10) are transformed to the global coordinates as

$$\Delta \mathbf{f}^a = \mathbf{T} \Delta \mathbf{f}^{a*} \quad \mathbf{T} = \begin{bmatrix} \cos \theta & -\sin \theta & 0 \\ \sin \theta & \cos \theta & 0 \\ 0 & 0 & 1 \end{bmatrix} \quad (11)$$

The internal force vector at the two nodes of the element can then be solved in the global coordinates as

$$\mathbf{f}_{n+1}^a = \mathbf{f}_n^a - \Delta \mathbf{f}^a \cdot \mathbf{e}_{n+1} \quad \text{and} \quad \mathbf{f}_{n+1}^b = \mathbf{f}_n^b + \Delta \mathbf{f}^b \cdot \mathbf{e}_{n+1} \quad (12)$$

## 2.2 VFIFE method for RTHS

Two groups of mass particles in the numerical substructure for RTHS. One group consists of general particles and the other is composed of particles at the interface associated with the experiment substructure. For particles of the interface, their internal force vector  $\mathbf{f}$  in Eq. (1) consists of two parts:  $\mathbf{f}_1$  from elemental force calculated in Section 2.1, and  $\mathbf{f}_2$  from experimental measurement. On the contrary, for general particles,  $\mathbf{f}$  is  $\mathbf{f}_1$ . Thus, the equations of motion (EOMs) of the entire RTHS system are in two forms: one for the general particles and the other for particles of the interface as

$$\mathbf{M}\ddot{\mathbf{u}} = \mathbf{F} - \mathbf{f}_1 \quad (13)$$

$$\mathbf{M}\ddot{\mathbf{u}} = \mathbf{F} - \mathbf{f}_1 - \mathbf{f}_2 \quad (14)$$

For the CDM, the critical integration time step  $h_c$  (Bathe 2006) can be obtained as

$$h_c = \frac{2}{\omega_n} = \frac{T_n}{\pi} \quad (15)$$

where  $\omega_n$  and  $T_n$  are the highest natural frequency and period of the structure.

In VFIFE,  $h_c$  is approximately taken as the first axial natural frequency  $\omega_{ele}$  (Pilkey 1978) of a segment obtained for fixed-fixed boundary condition as

$$\omega_n = \omega_{ele} = \frac{\pi}{l} \sqrt{\frac{E}{\rho}} = \frac{\pi c}{l} \quad (16)$$

$$h_c = \frac{2l}{\pi c}$$

where  $E$ ,  $\rho$ ,  $l$ , and  $c$  are the Young's modulus, mass density, segment length, and the propagation speed of the elastic wave, respectively. In the present VFIFE with CDM, the integration time step  $h$  is chosen using Eq. (16).

## 3. FPGA PLATFORM FOR VFIFE-BASED PARALLEL RTHS

### 3.1 Application of FPGA to RTHS

The FPGA is a kind of reprogrammable silicon chip with a large number of CLBs. With these prebuilt CLBs, developers can easily configure an FPGA chip to implement the functionality of custom hardware by programming the interconnections between them. In addition to CLBs, an FPGA chip also contains kinds of blocks with specified functions. With CLBs and the blocks, custom hardware integrated with different programs can be designed with the FPGA. Compared with other two electronics, multi-core central processing unit (CPU) and graphic processing unit (GPU), which are also widely used in the field of parallel computing, FPGA has two crucial advantages in

RTHS: 1) FPGA is better deterministic timing with considerably smaller latencies; 2) FPGA can connect to any other device via almost any interface.

Moreover, the FPGA can nowadays be easily designed in LabVIEW by graphical programming, which is very similar to the way in MATLAB/SIMULINK. Compared with a conventional developing tool, Verilog-HDL, the graphical programming is easier and more suited to researchers in civil engineering with limited technical background in electronics. Thus programs for numerical simulation, real-time control, and data acquisition can be easily integrated on a single FPGA-based device in the uniform developing environment of LabVIEW.

### 3.2 Parallel computations of VFIFE model on FPGA

The displacement prediction and element force evaluation can be performed in parallel for each particle (or particle group) as well as for each element (or element group) based on previous introduction. Fig. 2 depicts the parallel computation in the proposed parallel VFIFE analysis for the numerical substructure, where the particles and elements in VFIFE model are respectively divided into  $n$  and  $m$  groups.

For each particle and element group, the programs for displacement prediction and element force evaluation are designed with a group of CLBs on FPGA. The programs designed by the CLBs will finally be executed in the form of logic circuits on the FPGA. The speeds of displacement prediction and element force evaluation described in Fig. 2 are hence accelerated  $n$  and  $m$  times, respectively.

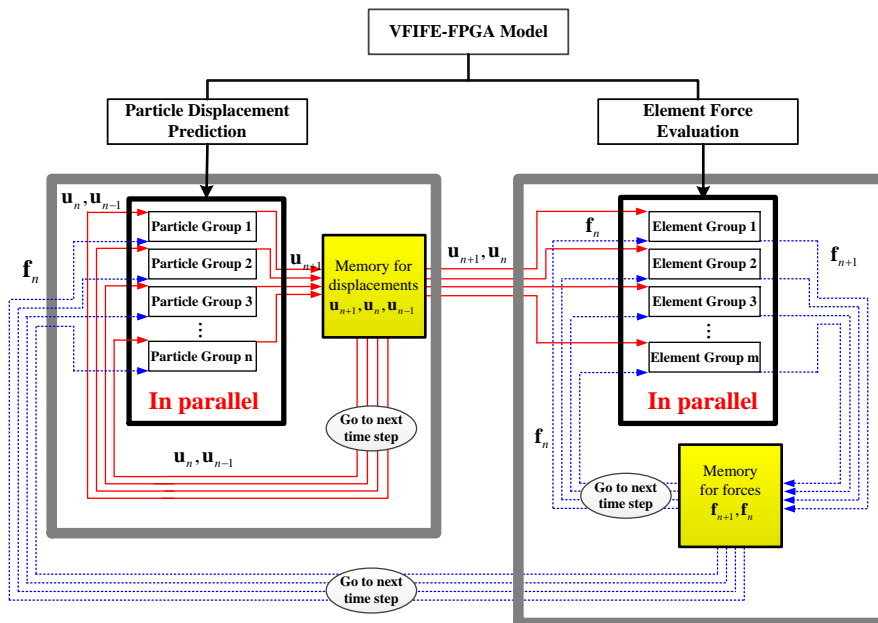


Fig. 2 Parallel computations for particle displacements and element forces in VFIFE-FPGA model

### 3.3 Parallel computing performance on FPGA

A simply supported beam, subjected to a step force at the mid-point, was introduced to evaluate the performance of parallel computation on the FPGA in Fig. 3. The structural properties of this case are listed in Tab. 1.

Considering the inherent damping in the structure, a damping force  $\mathbf{f}_d$  at each particle is added as

$$\mathbf{M}\ddot{\mathbf{u}} = \mathbf{F} - \mathbf{f} - \mathbf{f}_d \quad (17)$$

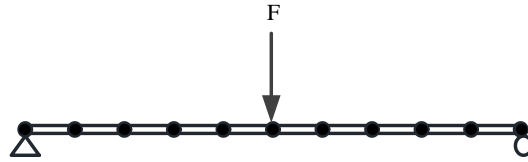


Fig. 3 Schematic of a simply supported beam

Tab. 1 Structural properties of the simply supported beam

| Parameters of the beam  | Values                             |
|-------------------------|------------------------------------|
| Mass density ( $\rho$ ) | 50 kg/m <sup>3</sup>               |
| Area ( $A$ )            | 0.125 m <sup>2</sup>               |
| Length ( $L$ )          | 4 m                                |
| Young's modulus ( $E$ ) | 10 <sup>3</sup> kN/m <sup>3</sup>  |
| Inertial moment ( $I$ ) | 2.6×10 <sup>3</sup> m <sup>4</sup> |
| Step force ( $F$ )      | 10 N                               |

In VFIFE, Rayleigh damping can be used by element-level mass and stiffness matrices as

$$\mathbf{f}_d = \alpha\mathbf{M}\dot{\mathbf{u}} + \beta\mathbf{K}\dot{\mathbf{u}} \quad (18)$$

where  $\mathbf{M}$  and  $\mathbf{K}$  are the mass and stiffness matrix of the element, and  $\alpha$  and  $\beta$  can be obtained as (Clough 1975)

$$\begin{bmatrix} \alpha \\ \beta \end{bmatrix} = 2 \frac{\omega_i \omega_j}{\omega_j^2 - \omega_i^2} \begin{bmatrix} \omega_j & -\omega_i \\ -1/\omega_j & 1/\omega_i \end{bmatrix} \begin{bmatrix} \xi_i \\ \xi_j \end{bmatrix} \quad (19)$$

where  $\omega_i$  and  $\omega_j$ ,  $\xi_i$  and  $\xi_j$  are two natural frequencies and modal damping ratios of structure, respectively. In particular, the damping force  $\mathbf{f}_{d,k}$  in linear structural system associated with the elemental stiffness in Eq. (17) is approximated as

$$\mathbf{f}_{d,k} = \beta\mathbf{K}\dot{\mathbf{u}}_n = \beta\dot{\mathbf{f}}_n \approx \beta \frac{\mathbf{f}_n - \mathbf{f}_{n-1}}{h} \quad (20)$$

In this case, the damping ratios were considered the same as 2.5%, and the first two modal frequencies were identified as 1.99 Hz and 7.81 Hz. The values of  $\alpha$  and  $\beta$  are obtained at 0.08 and 0.005, respectively.

The beam was modeled with 11 mass particles and 10 plane beam elements. The

critical time step given by Eq. (16) was  $1.8 \times 10^{-3}$  s with the first axial natural frequency  $\omega_{ele}$  of 1110.72 rad/s. Thus, a time step of  $10^{-3}$  s was chosen. The dynamic response at the middle of the beam is shown in Fig. 4. The results of the proposed method fit well with ANSYS results. The difference between the two results was quantified with an index of the root mean square (RMS) error norm, as

$$RMS \text{ error norm} = \sqrt{\frac{\frac{1}{N} \sum_{i=1}^N [d_i - x_i]^2}{\frac{1}{N} \sum_{i=1}^N [d_i]^2}} \quad (21)$$

where  $N$  is the number of time steps; result of ANSYS and VFIFE are taken as  $d_i$  and  $x_i$  used as reference and to be compared. The RMS error norm is found as 0.18%.

To further verify Equation (18-20), the damping force of the mid-point in vertical direction was respectively calculated by FE and VFIFE method. Fig. 5a shows that the proposed method can agree well with FE method. According to the results in Fig. 5b, the dissipate energy by VFIFE method reasonably fits the result of FE method.

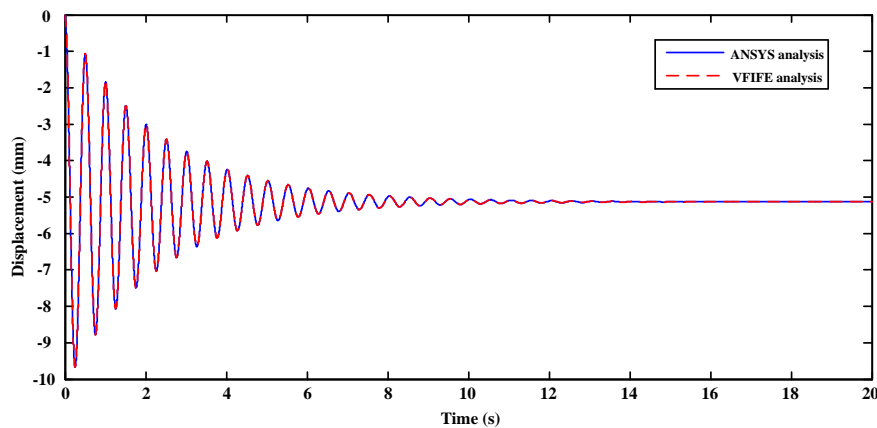


Fig. 4 Mid-point displacement of a beam under a step load

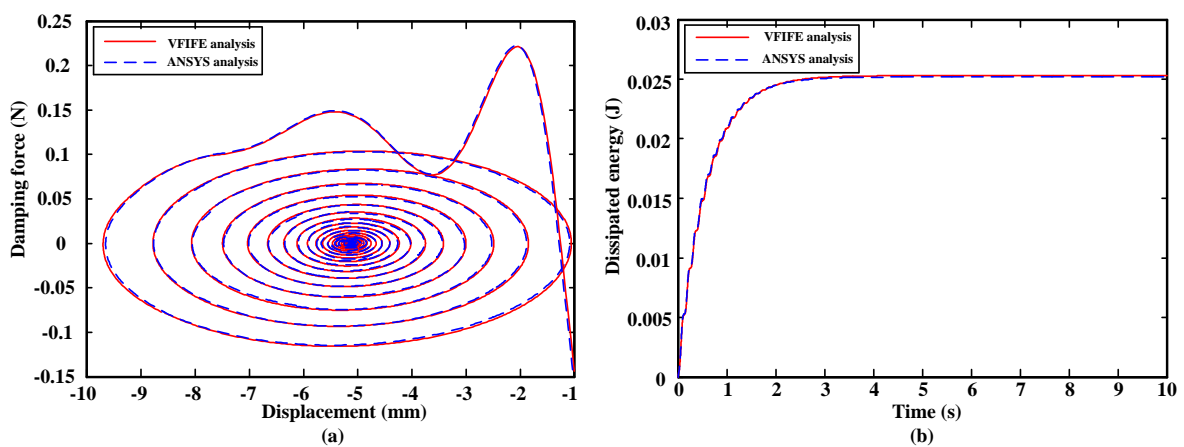


Fig. 5 Dissipated energy of the mid-point of a beam due to damping

Moreover, the simply supported beam was artificially divided into 101 particles and 100 elements to further investigate the performance of the parallel VFIFE analysis using FPGA. The particles and elements of the beam were grouped into the same numbers, from 1 to 15, for the sake of simplicity. The computation time taken for these different examples to run a single time step is described in Fig. 6.

It can be found that the computation time taken for each step decreases almost proportional to the increasing number of the groups (threads) in the parallel computation. The number of the parallel threads shall be selected considering the required time step in RTHS and the available sources in the FPGA chip.

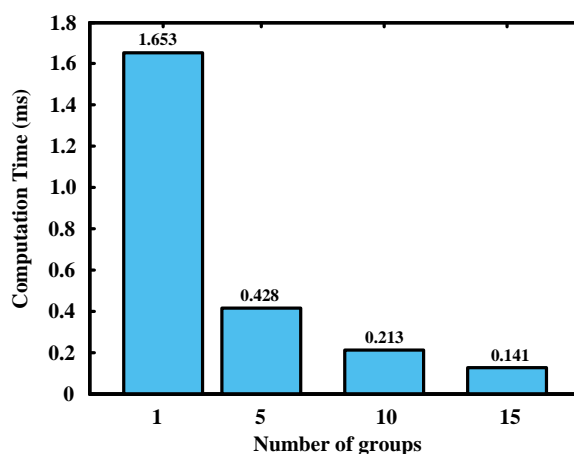


Fig. 6 Computation time versus the number of groups for a single time step

#### 4. VERIFICATION OF FPGA-BASED PARALLEL RTHS PLATFORM

##### 4.1 System design of RTHS based on FPGA

To design the proposed parallel RTHS platform, three components: a laptop, an FPGA-based device, and a loading system, are needed. Of these, the FPGA-based device is the major focus of this study. All programs, numerical simulation, real-time control, and data acquisition, were integrated into it, which can be divided into two parts, preprocessing and generating a real-time solution. The preprocessor is used to initialize the program and read the input parameters. The solution consists of eight steps as listed in Fig. 7. All these steps are programmed in a sequential manner and carried out one by one. Fig. 7 shows the framework of this RTHS platform in detail.

The timing control function Loop Timer Express VI (LTEV), provided by LabVIEW FPGA module, is used to ensure real-time solution on the FPGA. As shown in Fig. 8, if the run time of the program ( from steps 2 to 8) is less than a predefined time step, the LTEV makes the solution process wait until the total time is equal to the prescribed time step. It is not difficult for the FPGA to accurately implement the program at a fixed time step, since it can achieve a time resolution of up to 25 nanoseconds.

The program on FPGA was first designed as an FPGA Virtual Instrument (VI) of LabVIEW on the laptop. The LabVIEW FPGA compiler was then used to translate the FPGA VI into a bit-stream data file. A HOST VI was used to maintain communication with the FPGA VI by DMA to implement human-computer interaction. It allows users to monitor the experimental data in real time during the test.

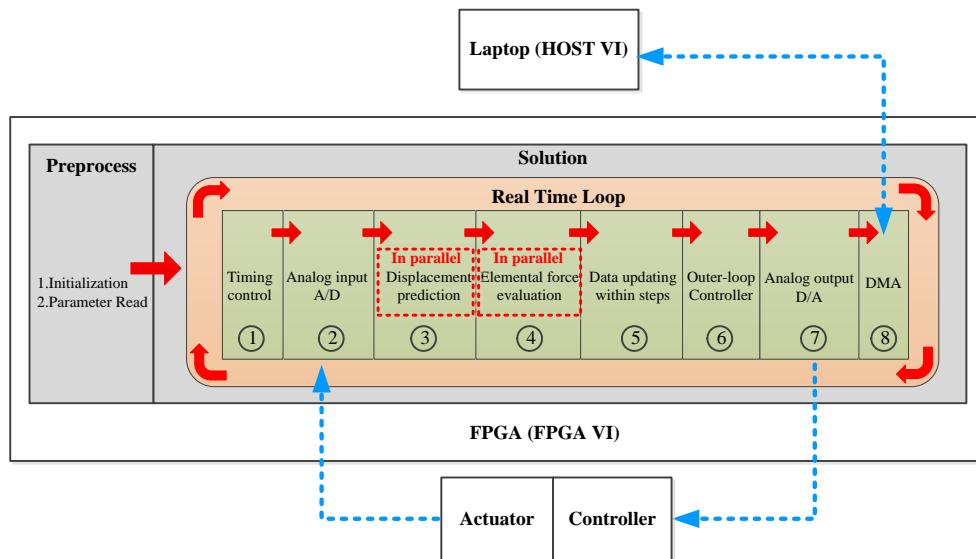


Fig. 7 Framework of the proposed parallel FPGA-based platform

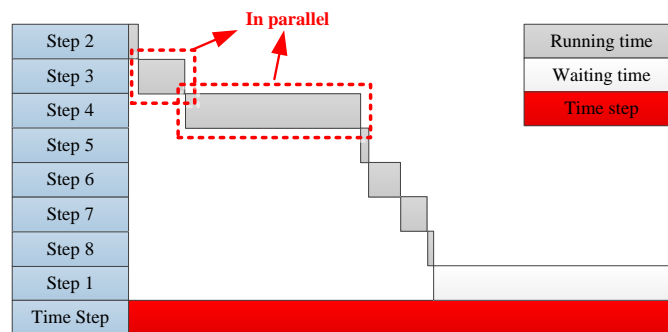


Fig. 8 Deterministic timing control of RTHS on FPGA

#### 4.2 Experimental verification of VFIFE-based RTHS

To verify the performance of the proposed RTHS platform, a simple RTHS was conducted. The numerical substructure used was a three-story structure considering the horizontal DOFs. Its structural properties are shown in Tab. 2. The natural frequencies of the structure were respectively 0.76, 2.02 and 2.72 Hz. The structural inherent damping was ignored. A step force of 0.5 kN was horizontally applied to the first floor of the structure. The time step was 0.001s. The stiffness along the horizontal direction was calculated at 16.519 kN/m. An overview of the structure is shown in Fig. 9.

Tab. 2. Structural properties of the test structure

| Floor No. | Story Stiffness, K(kN/m) | Floor Mass, M (kg) |
|-----------|--------------------------|--------------------|
| 1         | 42                       | 483.93             |
| 2         | 42                       | 483.93             |
| 3         | 35                       | 241.96             |

The calculated displacement imposed to the linear spring was applied using a fatigue-testing machine housing a uniaxial dynamic actuator of 50 kN at the Civil Lab in

Zhejiang University during the RTHS. A USB 7856R was used as the FPGA-based device and connected to the laptop with a universal serial bus cable. The converters on the FPGA chip can realize the conversion between analog and digital signals during the RTHS. The USB 7856R issued the FPGA output signals to the PID controller through the connection box, SCB-68, to control the actuator. The entire RTHS platform is shown in Fig. 10.

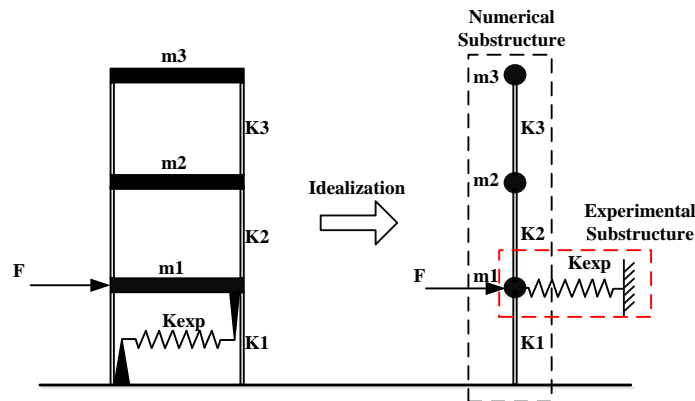


Fig. 9 Overview of the test structure

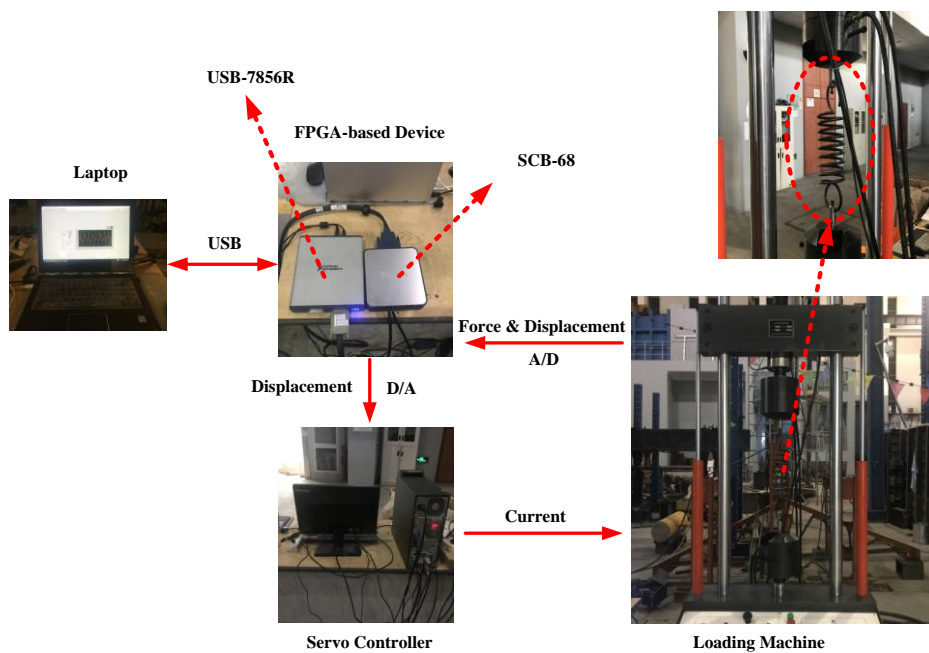


Fig. 10 Experimental configuration of RTHS

The dynamics of the hydraulic actuator are always troublesome and introduce a time lag to the loading system, which can lead to instability and divergence. Hence, an outer loop controller was needed to process the displacement signals before they were sent to the servo controller. A model-based feed-forward feedback controller (Phillips 2012) was used.

The tracking performance of the actuator with the linear spring and the chirp signal, at a range of 0.2 Hz-10 Hz, is presented in Fig. 11. The RMS error norms of the

tracking result decreased from 31.35% to 5.84% by employing the outer-loop controller.

As the present RTHS case was simple with a linear experimental substructure, the entire structure could be also analyzed by pure numerical methods. Thus, the structural response was computed using VFIFE and the conventional FE method in ANSYS. The displacements of the first floor obtained along the horizontal were compared in Fig. 12. The result of RTHS incorporating VFIFE was found to be almost identical to those of two analysis results.

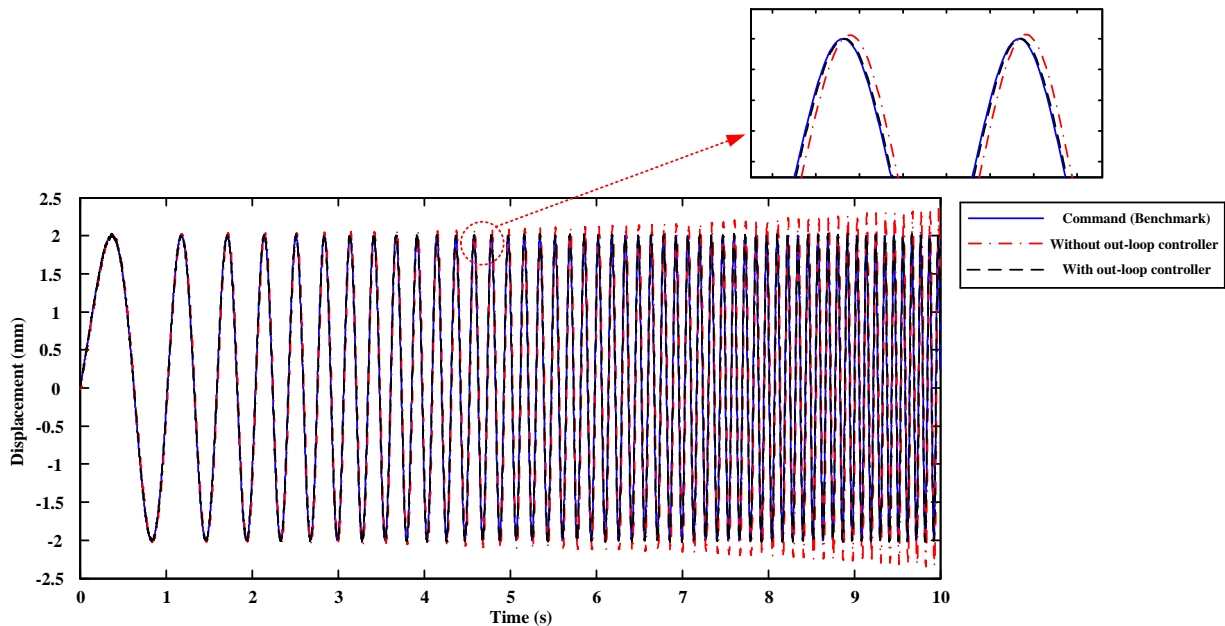


Fig. 11 Tracking performance of the actuator on chirp signal

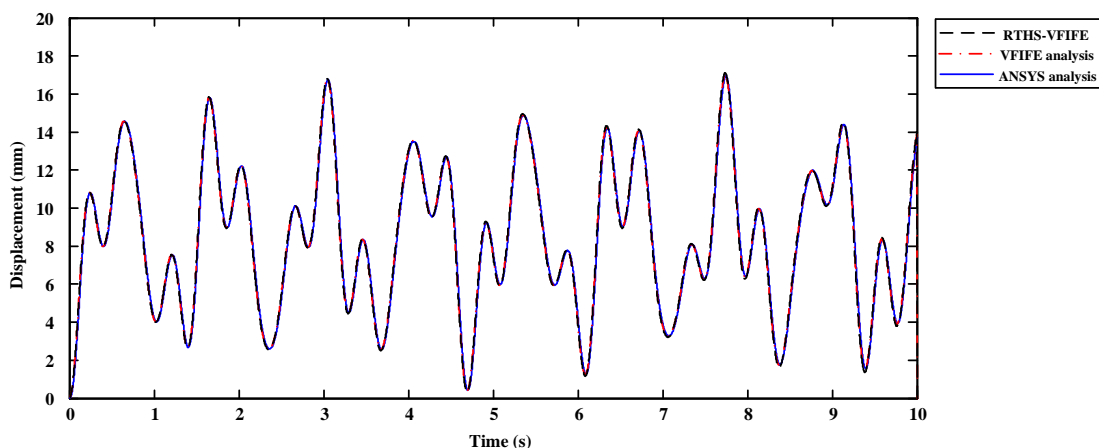


Fig. 12 Comparison of the results obtained by ANSYS, VFIFE and RTHS

#### 4.3. Verification of a virtual parallel RTHS on a cable-damper system

Cables used in long span bridges are prone to vibration induced by the connected structures and weather, and many researches have been taken to mitigate the cable vibration by installing external dampers (Johnson 2007, Duan 2005, Chen 2004, Lu 2017). The application of RTHS to evaluate the performance of the dampers will bring

much convenience comparing to a conventional field test. Thus, a virtual RTHS was conducted in this paper to further verify the performance of the proposed parallel RTHS platform. A cable, J-26, of The Second Jiaojiang Bridge, in Taizhou City, Zhejiang Province, China, was taken as a numerical substructure. The cable was divided into 51 mass particles and linked by 50 3D cable elements as in Fig. 13. To accelerate the speed of the numerical simulation in this virtual VFIFE-based RTHS, the particles and elements were divided into groups of three. The structural properties of the cable are shown in Tab. 3.

Tab. 3 Structural properties of Stay Cable J-26

| Parameters of the cable                    | Values                |
|--|-----------------------|
| Mass per unit ( $\rho$ )                   | 100.8 kg/m            |
| Cable length ( $L$ )                       | 255.47m               |
| Axial rigidity ( $EA$ )                    | $2.35 \times 10^6$ kN |
| Cosine of the slope angle ( $\cos\theta$ ) | 0.9137                |
| Pre-tension ( $T$ )                        | 6261 kN               |

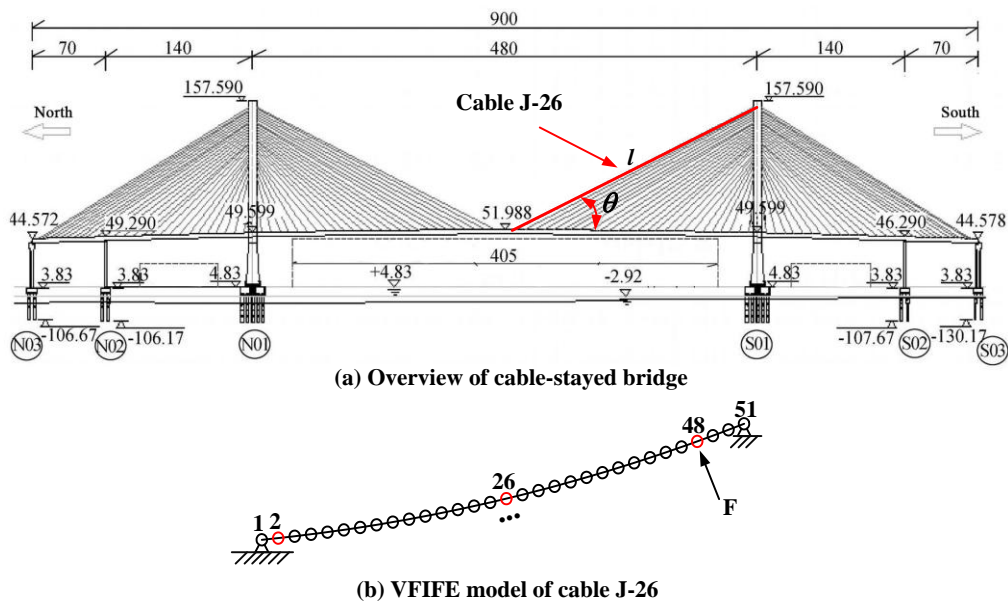


Fig. 13 Schematic of the stay cable in The Second Jiaojiang Bridge

Before starting the virtual RTHS, a pure numerical simulation of the cable response was conducted under an impact load of 1kN (lasting 1 second) applied perpendicularly to the cable at Node 48. The displacement at the mid-point of the cable was calculated by parallel VFIFE method on FPGA which can fit very well with ANSYS shown in shown in Fig. 14. Responses were also computed for various numbers of element discretization from 10 to 40. ANSYS result with 50 elements was considered as a reference. The natural frequencies of the cable were obtained by fast Fourier transform analysis on the calculated displacement at Node 2 near the lower support. The frequencies were very close to those obtained by ANSYS as shown in Tab. 4.

Tab. 4 Natural frequencies obtained by different methods (in Hz)

| Modes | ANSYS | VFIFE | Modes | ANSYS | VFIFE |
|-------|-------|-------|-------|-------|-------|
| 1     | 0.5   | 0.5   | 6     | 2.94  | 2.94  |
| 2     | 0.98  | 0.98  | 7     | 3.43  | 3.42  |
| 3     | 1.47  | 1.48  | 8     | 3.92  | 3.9   |
| 4     | 1.96  | 1.97  | 9     | 4.41  | 4.38  |
| 5     | 2.45  | 2.45  | 10    | 4.91  | 4.89  |

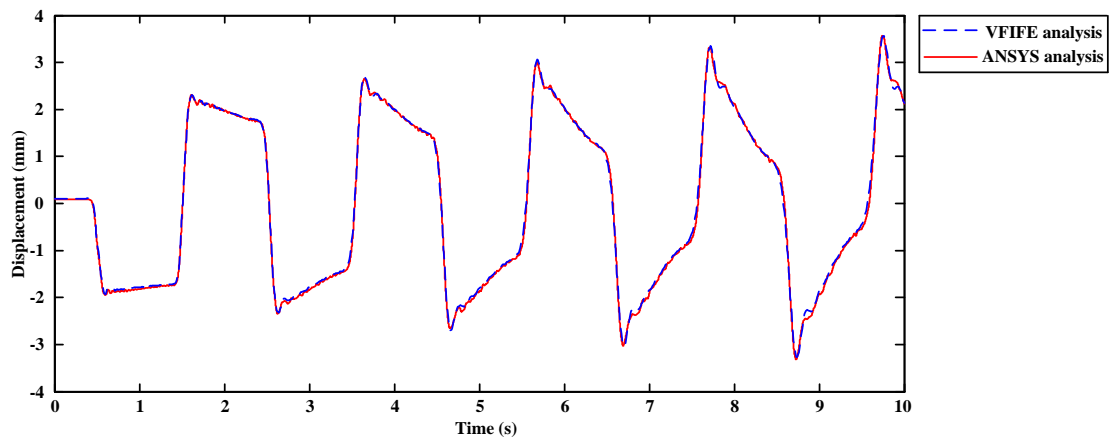


Fig. 14 Comparison of the mid-point responses obtained by VFIFE and ANSYS

In this virtual RTHS, a viscous damper located at Node 2 was used as experimental substructure for simplicity. For the servo hydraulic system in this virtual RTHS, a transfer function between the input displacement  $u$  and measured displacement  $x$  was employed to simulate the dynamics of the actuator. It was adopted from references (Carrion 2007, Qian 2014) as

$$G_{xu} = \frac{b}{a_4s^4 + a_3s^3 + a_2s^2 + a_1s + a_0} \quad (22)$$

where  $a_i (i=0,1,2,3,4)$  and  $b$  are relevant to the parameters listed in Tab. 5. The values of the servo hydraulic system parameters were taken from Carrion (2007), and the properties of the viscous damper were assumed as:  $m_f=0$ ,  $k=0$ ,  $c_f=0.3\text{kN}\cdot\text{s}/\text{mm}$ . The transfer function was obtained as

$$G_{xu} = \frac{71901.6}{s^3 + 303.956s^2 + 828.55s + 71901.6} \quad (23)$$

and implemented in discrete form to simulate the actuator dynamics. The entire virtual RTHS system was designed on FPGA. The block diagram is presented in Fig. 15.

Tab. 5 Definitions of parameters of the servo hydraulic system

|            |                            |           |                           |
|------------|----------------------------|-----------|---------------------------|
| $K_{prop}$ | Inner-loop controller gain | $\beta_e$ | Effective bulk modulus    |
| $K_q$      | Valve gain                 | $\tau_v$  | Servo valve time constant |
| $K_c$      | Total pressure coefficient | $m_t$     | Mass of the specimen      |
| $A$        | Piston area                | $k$       | Stiffness of the specimen |
| $V_t$      | Volume of fluid            | $c_t$     | Damping of the specimen   |

Without timing control by the LTEV, it took 44.06 s for the parallel VFIFE analysis to simulate the cable response for 150 s with a time step of 0.001 s. However it took 283 s for the ANSYS analysis. The LTEV slowed down the program and made it run at a fixed time interval of 0.001 s to match the predetermined time step. A sinusoidal excitation of  $F=1000\sin(\pi t)$ , at the first-order natural frequency of the cable, was applied perpendicularly to the cable at Node 48. The cable response at mid-point obtained by the RTHS was compared with Galerkin method (Johnson 2007) and ANSYS in Fig. 16. The result by the proposed parallel RTHS was found to be very close to the ANSYS result with a RMS error of 4.37%. However, the result by the Galerkin method was a little bit off from the ANSYS result with a RMS error of 12.6%. This might have obtained owing to the difference in assumptions regarding cable sag. Differing from the Galerkin method of introducing a parameter based on the assumption of parabola (Johnson 2007), ANSYS and VFIFE obtain cable sag by calculating the shape of the cable under gravity in advance.

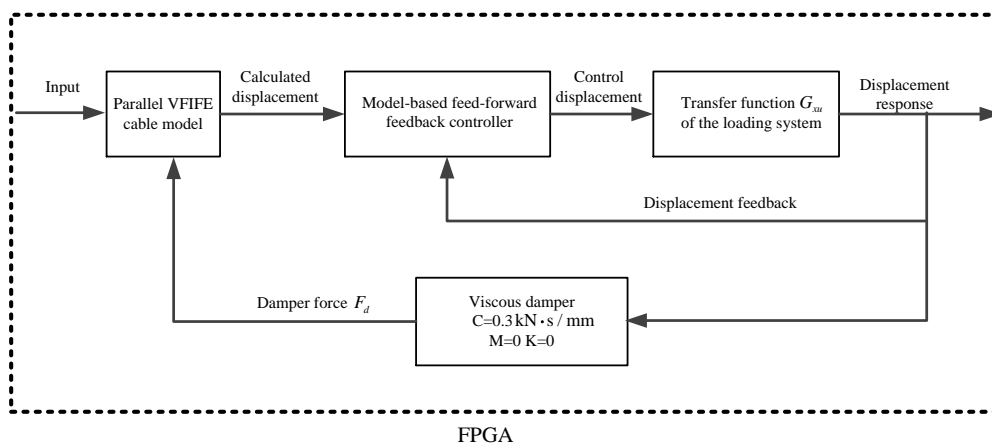


Fig. 15 Block diagram of the virtual RTHS on FPGA

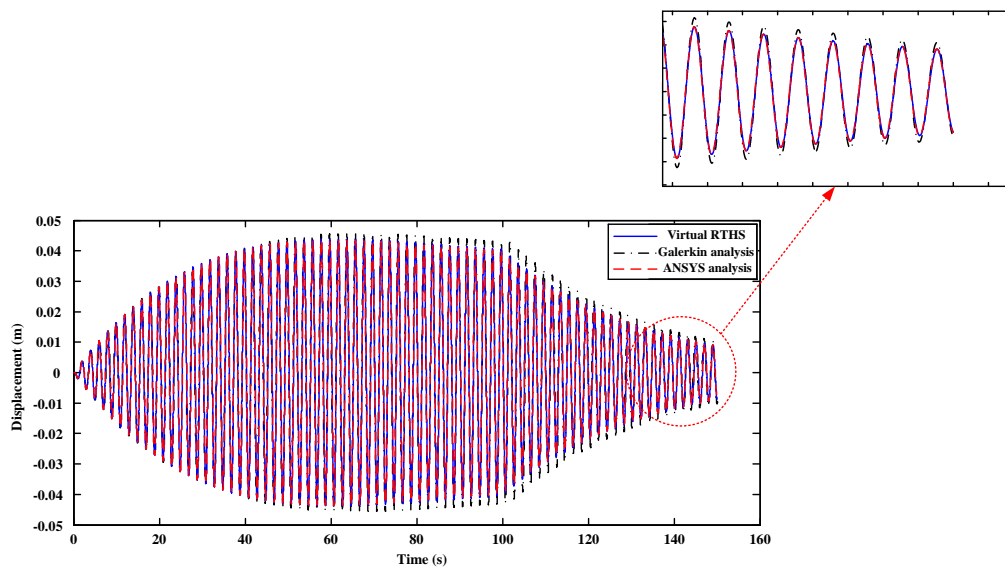


Fig. 16 Comparison of the results of the virtual RTHS with those of analysis

## 5. CONCLUSIONS

A parallel real-time hybrid simulation (RTHS) platform is proposed based on the vector form intrinsic finite element (VFIFE) method and the field-programmable gate array (FPGA) chip for the fast execution of RTHS with numerical substructures containing a large number of DOFs. The results obtained from two example cases are summarized as follows:

1. The proposed parallel platform can well integrate the numerical simulations, real-time control, and data acquisition on a single FPGA-based device. The capability of the platform to coordinate the data communication between two substructures in RTHS is fully verified.

2. The proposed FPGA-based parallel platform has shown its great potential to conduct a RTHS with a numerical substructure containing a large number of DOFs, with the fast computation and deterministic timing control.

3. Experiment on a three-story building structure with a linear spring shows that the proposed VFIFE-based RTHS performs very well. The model-based feed-forward feedback controller introduced to the actuator can improve the tracking performance from 31.4% error to 5.9% error in RMS-level.

4. Virtual parallel RTHS on a cable-damper system with 147 DOFs shows that dynamic response of the cable can be simulated accurately with a RMS error of 4.4% in comparison with the result by ANSYS analysis.

Future research works are suggested regarding the proposed VFIFE-based parallel RTHS platform.

1. The present VFIFE method is based on conditionally stable, unconditional stable numerical schemes may be employed in the future study.

2. More refined and complicated structural behaviors such as the hysteretic model (Yu 2016) shall be considered in the numerical substructure for the VFIFE-based RTHS.

## ACKNOWLEDGEMENTS

This work is supported by National Natural Science Foundation of China (U1709216, 51522811, 51478429, and 90915008), Zhejiang Provincial Natural Science Foundation of China (LR13E080001, LQ15E080008) and the Fundamental Research Funds for the Central Universities (2015XZZX004-28).

## REFERENCES

- Ashasi-Sorkhabi A.(2015), "Implementation, Verification and Application of Real-time Hybrid Simulation", *Ph.D thesis*.
- Bathe, K.J.(2006), *Finite element procedures*, Klaus-Jurgen Bathe.
- Carrion, J.E. and Spencer, B.F.(2007), "Model-based strategies for real-time hybrid testing", *Newmark Structural Engineering Laboratory Report Series NO.006*. University of Illinois at Urbana-Champaign: Urbana, IL.
- Chen, C., Ricles, J.M., Marullo, T.M. and Mercan, O.(2009), "Real-time hybrid testing using the unconditionally stable explicit CR integration algorithm", *Earthquake Engineering and Structural Dynamics*, **38**(1), 23-44.
- Chen, Z.Q., Wang, X.Y., Ko, J.M., Ni, Y.Q., Spencer, B.F., Yang, G. and Hu, J.H.(2004), "MR damping system for mitigating wind-rain induced vibration on Dongting Lake Cable-Stayed Bridge", *Wind & structures*, **7**(5), 293-304.
- Clough, R.W. and Penzien, J.(1975), *Dynamics of Structures*, New York McGrawHill Inc..
- Duan, Y.F., He, K., Zhang, H.M., Ting, E.C., Wang, C.Y., Chen, S.K. and Wang, R.Z.(2014), "Entire-Process Simulation of Earthquake-Induced Collapse of a Mockup Cable-Stayed Bridge by Vector Form Intrinsic Finite Element (VFIFE) Method", *Advances in Structural Engineering*, **17**(3), 347-360.
- Duan, Y.F., Ni, Y.Q. and Ko, J.M.(2005), "State-derivative feedback control of cable vibration using semi-active MR dampers", *Computer-Aided Civil and Infrastructure Engineering*, **20** (6), 431-449.
- Duan, Y.F., Wang, S.M., Wang, R.Z., Wan, C.Y., and Ting, E.C.(2017), "Vector form intrinsic finite element based approach to simulate crack propagation", *Journal of Mechanics*, **33**(6), 797-812.
- Ferry, D., Maghareh, A., Bunting, G., Prakash, A., Agrawal, K., Gill, C., Lu, C. and Dyke, S.J.(2014), "On the performance of a highly parallelizable concurrency platform for real-time hybrid simulation", *The Sixth World Conference on Structural Control and Monitoring*.
- Horiuchi, T., Inoue, M., Konno, T., and Namita, Y.(1999), "Real-time hybrid experimental system with actuator delay compensation and its application to a piping system with energy absorber," *Earthquake Engineering and Structural Dynamics*, **28**(10), 1121-1141.
- Johnson, E.A., Baker, G.A., Spencer, B.F. and Fujino, Y.(2007), "Semiactive Damping of Stay Cables", *Journal of Engineering Mechanics*, **133**(1),1-11.

- Johnson, E.A., Christenson, R.E. and Spencer, B.F.(2003), "Semiactive damping of cables with sag". *Computer-Aided Civil and Infrastructure Engineering*, **18**(2), 132-146.
- Jung, S. and Kim, S.S.(2007), "Hardware implementation of a real-time neural network controller with a DSP and an FPGA for nonlinear systems", *IEEE Transactions on Industrial Electronics*, **54**(1), 265-271.
- Lu, L., Duan, Y.F., Spencer, B.F., Lu, X. and Zhou, Y.(2017), "Inertial mass damper for mitigating cable vibration", *Structural Control and Health Monitoring*, **24**, e1986.
- Mercan, O. and Ricles, J.M.(2009), "Experimental studies on real-time testing of structures with elastomeric dampers", *Journal of Structural Engineering*, **135**(9), 1124-1133.
- Nakashima, M., Kato, H., and Takaoka, E. (1992), "Development of real-time pseudo dynamic testing", *Earthquake Engineering and Structural Dynamics*, **21**(1), 79-92.
- Phillips, B.M. and Spencer, B.F.(2012), "Model-based feed-forward feedback actuator control for real-time hybrid simulation", *Journal of Structural Engineering*, **139**(7), 1205-1214.
- Pilkey, W.D., and Chang, P.Y.(1978), "Modern Formulas for Statics and Dynamics: A Stress and Strain Approach", New York McGraw-Hill Inc..
- Qian, Y., Ou, G., Maghareh, A. and Dyke, S.J.(2014), "Parametric identification of a servo-hydraulic actuator for real-time hybrid simulation", *Mechanical Systems and Signal Processing*, **48**(1), 260-273.
- Ting, E.C., Shih, C., Wang, Y.K.(2004a), "Fundamentals of a vector form intrinsic finite element: Part I. Basic procedure and a plane frame element", *Journal of Mechanics*, **20**(2), 113-122.
- Ting, E.C., Shih, C. and Wang, Y.K.(2004b), "Fundamentals of a vector form intrinsic finite element: Part II. Plane solid elements", *Journal of Mechanics*, **20**(2), 123-132.
- Wang, R.Z., Tsai, K.C. and Lin, B.Z.(2011), "Extremely large displacement dynamic analysis of elastic-plastic plane frames", *Earthquake Engineering and Structural Dynamics*, **40**(13), 1515-1533.
- Wu, B., Xu, G., Wang, Q. and William, M.S.(2006), "Operator-splitting method for real-time substructure testing", *Earthquake Engineering and Structural Dynamics*, **35**(13), 293-314.
- Wu, T.Y. and Ting, E.C.(2008), "Large deflection analysis of 3D membrane structures by a 4-node quadrilateral intrinsic element", *Thin-Walled Structures*, **46**(3), 261-275.
- Lien, K.H., Chiou, Y.J., Wang, R.Z. and Hsiao, P.A.(2010), "Vector form intrinsic finite element analysis of nonlinear behavior of steel structures exposed to fire", *Engineering structures*, **32**(1), 80-92.
- Yu, Y., and Zhu, X.(2016), "Nonlinear dynamic collapse analysis of semi-rigid steel frames based on the finite particle method". *Engineering Structures*, **118**, 383-393.